

Magnetocaloric Effect of Two Gd-Based Frameworks

Bo-Liang Liu, Qiao-Fei Xu, La-Sheng Long * and Lan-Sun Zheng

Collaborative Innovation Center of Chemistry for Energy Materials, State Key Laboratory of Physical Chemistry of Solid Surfaces and Department of Chemistry, College of Chemistry and Chemical Engineering, Xiamen University, Xiamen 361005, China; 20520191151524@stu.xmu.edu.cn (B.-L.L.); 20520190154165@stu.xmu.edu.cn (Q.-F.X.); lszheng@xmu.edu.cn (L.-S.Z.)

* Correspondence: lslong@xmu.edu.cn

Abstract: Magnetic refrigeration material is the key to adiabatic demagnetization refrigeration technology. In this work, two magnetic refrigerants, $\text{Gd}_5(\text{C}_4\text{O}_4)(\text{HCOO})_3(\text{CO}_3)_2(\text{OH})_6 \cdot 2.5\text{H}_2\text{O}$ (**1**) and $\text{Gd}_2(\text{OH})_4\text{SO}_4$ (**2**), were prepared through hydrothermal reaction. Magnetic study reveals that their magnetic entropy changes are $24.8 \text{ J kg}^{-1} \text{ K}^{-1}$ for **1** and $15.1 \text{ J kg}^{-1} \text{ K}^{-1}$ for **2** at 2 K and 2 T, respectively. The magnetic entropy changes of **1** and **2** at $T = 2 \text{ K}$ and $\Delta H = 2 \text{ T}$ exceed most gadolinium hydroxyl compounds, indicating that magnetic refrigerants with large magnetic entropy changes at low magnetic fields can be obtained by introducing more weak magnetic exchange ligands to replace hydroxyl groups in gadolinium hydroxyl compounds.

Keywords: magnetocaloric effect; hydroxyl; cryogenic; magnetic refrigeration

1. Introduction

Since the magnetocaloric effect (MCE) of Fe and Ni was observed by Warburg and Weiss in 1881 [1] and 1917 [2], respectively, the adiabatic demagnetization refrigeration (ADR), which is based on the MCE, has gained extensive attention over the century, not only because it has the advantages of environmental friendliness and energy efficiency [3–5] but it is also a promising method to reach the subkelvin temperature region (below 1 K) without the use of rare ^3He gas [6,7]. Owing to the magnetic entropy changes ($-\Delta S_m$) of magnetic refrigerants being the driving force of ADR, a great many efforts have been made in the preparation of large MCE magnetic refrigerants in the past decades. Although some large MCE magnetic refrigerants, such as $\text{Gd}(\text{HCOO})_3$ [8], $\text{Gd}(\text{OH})_3$ [9], $\text{Gd}(\text{OH})\text{CO}_3$ [10], GdPO_4 [11] and GdF_3 [12], have been successfully obtained so far, on one hand, these compounds are already known and thus it is necessary to find new magnetic refrigerants with large MCE. On the other hand, although various Gd-based materials, such as inorganic salts [11–13], molecule-based clusters [14–20], inorganic metallic oxides [21–23] and coordination polymers [24–26], were selected as magnetic refrigerants in the past decades, few of them contain four different inorganic ligands and thus how the collaboration among these ligands affects their MCE remains unclear. Here we report syntheses and MCE of two magnetic refrigeration materials, namely, $\text{Gd}_5(\text{C}_4\text{O}_4)(\text{HCOO})_3(\text{CO}_3)_2(\text{OH})_6 \cdot 2.5\text{H}_2\text{O}$ (**1**) and $\text{Gd}_2(\text{OH})_4\text{SO}_4$ (**2**), of which compound **1** represents the very rare example of inorganic Gd-based compound formed by four different inorganic anions.

2. Results and Discussion

Compound **1** was synthesized through the hydrothermal reaction of gadolinium chloride hexahydrate with squaric acid in the mixed solvent of *N,N*-dimethylformamide (DMF) and water. Compound **2** was synthesized by the hydrothermal reaction of gadolinium nitrate hexahydrate with ammonium carbonate and sulfuric acid in aqueous solution. Powder X-ray diffraction (PXRD) patterns of the bulk sample **1** and **2** reveal that the experimental diffraction patterns are consistent with those simulated by the single crystal



Citation: Liu, B.-L.; Xu, Q.-F.; Long, L.-S.; Zheng, L.-S. Magnetocaloric Effect of Two Gd-Based Frameworks. *Inorganics* **2022**, *10*, 91. <https://doi.org/10.3390/inorganics10070091>

Academic Editors: Leonor Maria and Joaquim Marçalo

Received: 8 June 2022

Accepted: 23 June 2022

Published: 25 June 2022

Publisher's Note: MDPI stays neutral with regard to jurisdictional claims in published maps and institutional affiliations.



Copyright: © 2022 by the authors. Licensee MDPI, Basel, Switzerland. This article is an open access article distributed under the terms and conditions of the Creative Commons Attribution (CC BY) license (<https://creativecommons.org/licenses/by/4.0/>).

data (Figure S1, see the Supplementary Materials), demonstrating the purity of the bulk sample 1 and 2. Thermogravimetric analysis (TGA) under nitrogen atmosphere indicates the weight loss at 265 °C is 3.89% for 1, attributed to the loss of two and a half H₂O. The total weight loss of 29.78% corresponds well to the theoretical value of 30.31% when the residue is Gd₂O₃. Sample 2 has good thermal stability and can remain stable up to 350 °C. The weight loss of 7.29% matches well with that of 7.52% calculated by two H₂O at the temperature of 430 °C (Figure S2). Both the experimental PXRD patterns and TGA further confirm the purity of the bulk sample 1 and 2. The O atoms in the main structure are assigned to hydroxyl groups based on bond valence sum (BVS) calculations [27] and charge balance requirements (Tables S1 and S2).

Single crystal X-ray diffraction analysis shows that 1 and 2 crystallize in the monoclinic system with space groups $P2_1/c$ and $C2/m$, respectively (Figures S3 and S4). Crystal data and structural refinement details are shown in Table S3. The asymmetric unit of 1 consists of five Gd³⁺ ions, six OH[−] anions, two CO₃^{2−} anions, three HCOO[−] anions, one C₄O₄^{2−} anion and two and a half H₂O. Gd1 to Gd4 are all coordinated with four OH[−], one HCOO[−], two CO₃^{2−} and one C₄O₄^{2−} in monodentate mode. Gd5 is coordinated with two OH[−], two monodentate HCOO[−] and two CO₃^{2−} in chelated mode. Gd1 and Gd2 are in triangular dodecahedron geometry calculated by continuous shape measurements [28] (CShM). Gd3 and Gd4 are in square antiprism, while Gd5 is in biaugmented trigonal prism (Table S4). Figure 1a shows that four Gd³⁺ ions are linked by four OH[−], generating a [Gd₄(OH)₄]_n⁸ⁿ⁺ cubane. Four [Gd₄(OH)₄]_n⁸ⁿ⁺ cubanes centered by a Gd³⁺ ion through the connection of HCOO[−], CO₃^{2−} and OH[−] form a butterfly-shaped unit of [Gd₁₇(OH)₂₀(HCOO)₃(CO₃)₂]_n²⁴ⁿ⁺, as shown in Figure 1b. It is worth noting that the two cubanes on the left side of the butterfly-shaped unit are connected to the central Gd³⁺ through two HCOO[−] and one CO₃^{2−}, while these on the right side of the butterfly-shaped unit are connected to the central Gd³⁺ through one HCOO[−] and one CO₃^{2−}. Based on previous work, the ligands of CO₃^{2−} and HCOO[−] were generated from the decomposition of squaric acid in situ under hydrothermal conditions [29,30]. Adjacent butterfly-shaped units expand into a 2D layer of [Gd₅(OH)₆(HCOO)₃(CO₃)₂]_n²ⁿ⁺ through sharing edges, as shown in Figure 1c. The adjacent layers are pillared by squarate in a $\mu_4-\eta^1:\eta^1:\eta^1:\eta^1$ coordination mode, forming into a 3D framework of 1 (Figure 1d).

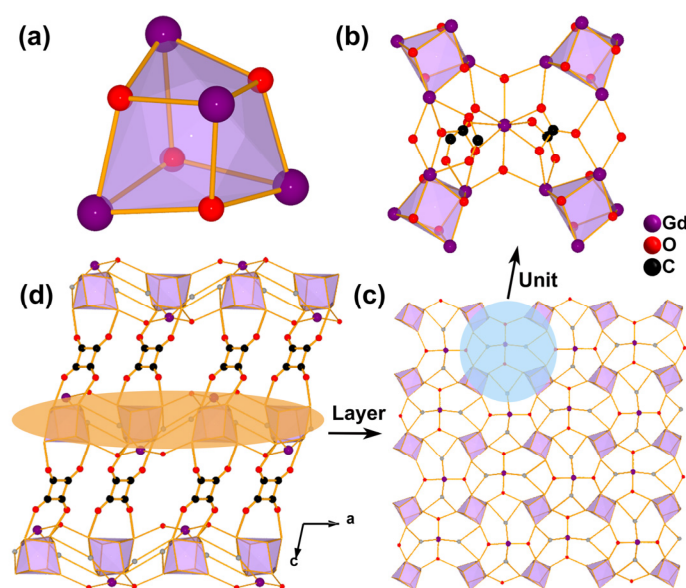


Figure 1. (a) [Gd₄(OH)₄]_n⁸ⁿ⁺ cubane; (b) Butterfly-shaped unit of [Gd₁₇(OH)₂₀(HCOO)₃(CO₃)₂]_n²⁴ⁿ⁺ in 1; (c) topology of the layer structure of [Gd₅(OH)₆(HCOO)₃(CO₃)₂]_n²ⁿ⁺ constructed by the butterfly-shaped units through sharing edges; (d) the 3D structure of 1 formed through the adjacent layer structures pillared by C₄O₄^{2−} in a $\mu_4-\eta^1:\eta^1:\eta^1:\eta^1$ coordination mode. Hydrogen atoms are omitted for clarity.

Compound **2** is a known compound [31,32], but its single crystal structure has not yet been obtained. The asymmetric unit of **2** contains half of one Gd^{3+} ion, one OH^- anion and a quarter of one SO_4^{2-} anion. The central Gd^{3+} is coordinated by six OH^- anions and two SO_4^{2-} anions in chelated mode in metabidiminished icosahedron geometry (Table S5). Figure 2a reveals that the Gd^{3+} ions are bridged by $\mu_3\text{-OH}^-$, forming a classic 2D layer of $[\text{Gd}_2(\text{OH})_4]_n^{2n+}$ as observed in $\text{Gd}(\text{OH})_2\text{Cl}$ [33]. The 3D framework can be viewed as the adjacent layers connected by sulfates in a $\mu_4\text{-}\eta^1:\eta^1:\eta^2:\eta^2$ coordination mode, as shown in Figure 2b. It was mentioned that although the 2D layer structure in **1** is very similar to that in $\text{Gd}(\text{OH})_2\text{Cl}$, the latter is in fact a 3D supramolecular network viewed as a connection of adjacent 2D layer structures through electrostatic interactions between Cl^- anions and $[\text{Gd}(\text{OH})_2]_n^{n+}$ layers.

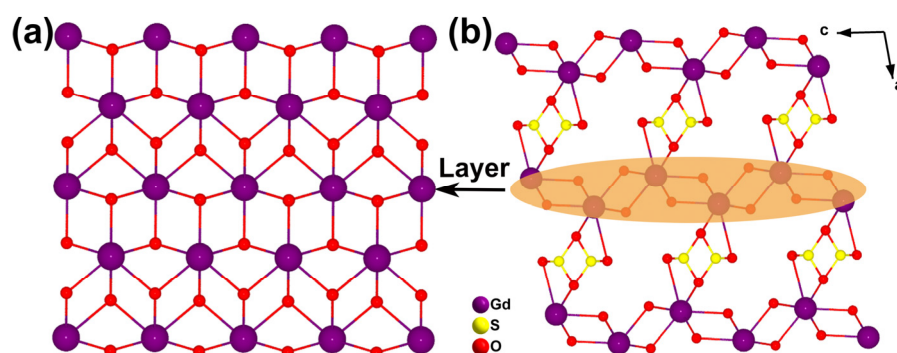


Figure 2. (a) The layer structure of $[\text{Gd}_2(\text{OH})_4]_n^{2n+}$; (b) the connection mode of SO_4^{2-} between adjacent layers in **2**. Hydrogen atoms are omitted for clarity.

The lengths of Gd–O bond in **1** and **2** range from 2.298(6) to 2.516(5) Å and 2.375(8) to 2.518(10) Å, and the Gd–O–Gd angles vary from 104.37(14) ~ 116.37(16)° and 92.9(5) ~ 110.8(4)°, respectively. The distances between Gd···Gd are 3.815(6) ~ 8.561(4) Å and 3.650(6) ~ 6.762(15) Å for **1** and **2** (Tables S6 and S7). The bond lengths and angles are comparable to those reported in $\text{Gd}(\text{OH})_2\text{Cl}$ [33].

Figure 3a illustrates the temperature-dependent magnetic susceptibility of **1** and **2** measured in a temperature range of 2 to 300 K under a direct current (dc) magnetic field of 1000 Oe. At room temperature, the values of $\chi_M T$ of **1** and **2** are 39.21 $\text{cm}^3 \text{K mol}^{-1}$ and 15.48 $\text{cm}^3 \text{K mol}^{-1}$, respectively, corresponding to the calculated theoretical values of 39.40 $\text{cm}^3 \text{K mol}^{-1}$ for five spin-only Gd^{3+} ions ($^8S_{7/2}$, $S = 7/2$, $g = 2$) and 15.48 $\text{cm}^3 \text{K mol}^{-1}$ for two Gd^{3+} ions. From 300 K to 100 K, the $\chi_M T$ values of the two compounds remain unchanged. Then, the $\chi_M T$ values decrease slowly till temperature continues to cool down to 25 K. Further decreasing the temperature, the $\chi_M T$ values start to decrease rapidly and reach 20.78 $\text{cm}^3 \text{K mol}^{-1}$ for **1** and 5.49 $\text{cm}^3 \text{K mol}^{-1}$ for **2** at 2 K. The rapid decreasing $\chi_M T$ vs. T curves indicate the existence of antiferromagnetic (AFM) interactions between adjacent Gd^{3+} ions in both **1** and **2**. Consistently, fitting the χ_M^{-1} vs. T data of **1** and **2** with the Curie–Weiss law gives $C = 39.57 \text{ cm}^3 \text{K mol}^{-1}$ and $\theta = -2.25 \text{ K}$ for **1** and $C = 15.71 \text{ cm}^3 \text{K mol}^{-1}$, $\theta = -2.78 \text{ K}$ for **2**. The negative Weiss constants further manifest the presence of antiferromagnetic coupling between Gd^{3+} ions of **1** and **2**. Figure S5 shows the isothermal magnetization data in applied magnetic field from 0 to 7 T in the temperature range from 2 to 10 K for **1** and **2**. The magnetization increases with the decrease of temperature at a given applied magnetic field and decreases with the decrease of magnetic field at a given temperature. At 2 K and 7 T, the magnetizations of the two samples approach the saturation values and reach 34.78 $\text{N}\mu_B$ for **1** and 13.93 $\text{N}\mu_B$ for **2**, which are consistent with the theoretical values of 35 $\text{N}\mu_B$ and 14 $\text{N}\mu_B$ calculated through five Gd^{3+} ions ($J = 7/2$, $L = 0$, $S = 7/2$) and two Gd^{3+} ions.

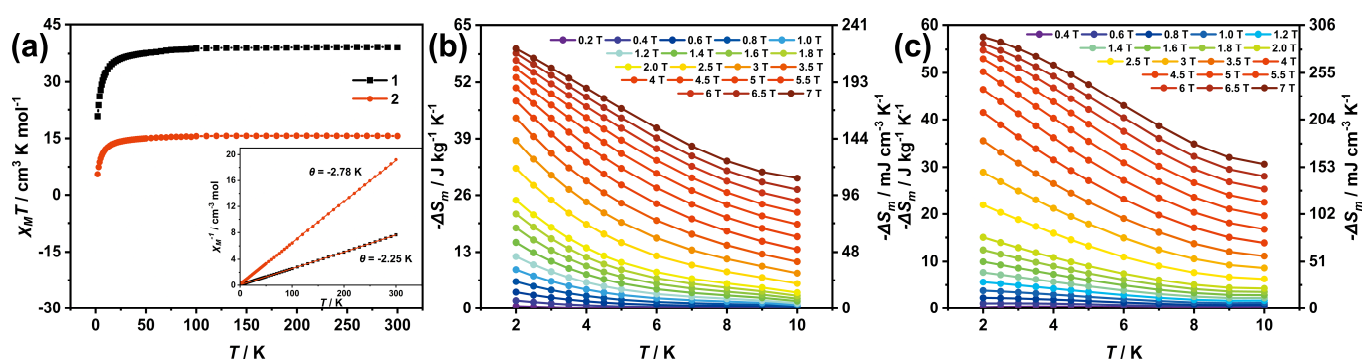


Figure 3. (a) Temperature dependence of $\chi_M T$ for **1** and **2** under a 1000 Oe magnetic field in the range of 2–300 K; inset: the χ_M^{-1} vs. T plot of **1** and **2** in the temperature range of 2–300 K. The red solid lines are the best-fit, according to the Curie–Weiss law; experimental $-\Delta S_m$ values of **1** and **2** for multiple temperatures and magnetic fields calculated from magnetization data: **1** (b); **2** (c).

Since **1** and **2** both have large mass ratio of metal to ligand, the experimental MCE of **1** and **2** was investigated by using multiple temperature data of magnetization to fit the Maxwell equation [34] below:

$$\Delta S_m(T)_{\Delta H} = \int [\partial M(T, H) / \partial T]_H dH \quad (1)$$

As shown in Figure 3b,c, the magnetic entropy changes ($-\Delta S_m$) of **1** and **2** increase monotonically with the decrease of temperature and the increase of magnetic field, reaching the maximum value of $59.8 \text{ J kg}^{-1} \text{ K}^{-1}$ ($221 \text{ mJ cm}^{-3} \text{ K}^{-1}$) and $57.6 \text{ J kg}^{-1} \text{ K}^{-1}$ ($293 \text{ mJ cm}^{-3} \text{ K}^{-1}$), respectively, at 2 K and 7 T.

For comparison, the theoretical $-\Delta S_m$ for **1** and **2** was also calculated by the equation $-\Delta S_m = nR \ln(2S + 1) / M_w$ [35,36], which shows that the $-\Delta S_m$ is $66.5 \text{ J kg}^{-1} \text{ K}^{-1}$ for **1** and $72.2 \text{ J kg}^{-1} \text{ K}^{-1}$ for **2**. Both the experimental MCE of **1** and **2** were obviously smaller than theoretical MCE of **1** and **2**; this is attributed to the existence of relatively strong antiferromagnetic interactions in **1** and **2**, which degrade the spin degeneracy causing the inability to obtain large magnetic entropy changes under limited magnetic field [37].

Table 1 lists the magnetic interactions and the magnetic entropy changes of some excellent magnetic refrigerants reported to date under the applied magnetic field of 2 T and 7 T. For comparison, the magnetic interactions and the magnetic entropy changes of some magnetic refrigerants containing OH^- group are also listed. Although the MCE of **1** and **2** at 7 T is significantly smaller than that of GdF_3 and $\text{Gd}(\text{OH})\text{CO}_3$, it is comparable to that of $[\text{Gd}_3(\text{CO}_3)(\text{OH})_6]\text{OH}$, $\text{Gd}(\text{OH})_3$ and $\text{Gd}(\text{OH})_2\text{Cl}$. It was mentioned that although the MCE of $\text{Gd}(\text{HCOO})_3$ at 7 T is obviously smaller than that of **1** and **2**, its MCE at 2 T is significantly larger than that of **1** and **2**. This result distinctly indicates that weak magnetic interaction favors to obtain large MCE magnetic refrigerants at low applied magnetic field. Because of the limitation of weight and high magnetic field interference in space missions, the magnetic field above 4 T cannot be generated properly [38], and commercial magnets such as NbTi [39] and NdFeB [40,41], can easily provide a magnetic field of 2 T. Except for $\text{Gd}(\text{OH})\text{CO}_3$, $\text{Gd}(\text{OH})_3$ and $\text{Gd}_4(\text{OH})_4(\text{SO}_4)_4(\text{H}_2\text{O})_4$, the magnetic entropy changes of other gadolinium hydroxyl compounds listed in Table 1 are all lower than that of **1** in low magnetic field. In combination with the composition of these compounds, this result indicates that magnetic refrigerants with large MCE at low fields can be obtained by introducing more weak magnetic exchange ligands to replace hydroxyl groups in gadolinium hydroxyl compounds, consistent with the fact that the MCE of $\text{Gd}(\text{OH})\text{CO}_3$ is significantly larger than that of $\text{Gd}(\text{OH})_3$. Based on the Table 1, the MCE of $\text{Gd}(\text{OH})_3$ larger than that of **1** is obviously related to the fact that its magnetic density is higher than that of **1**. Therefore, in order to obtain gadolinium hydroxyl compounds with large magnetic entropy changes, it is necessary to maintain high magnetic density of the gadolinium

hydroxyl compounds, in addition to introducing more weak magnetic exchange ligands to replace hydroxyl groups in gadolinium hydroxyl compounds. It was noted that although the mass magnetic entropy change of **1** ($24.8 \text{ J kg}^{-1} \text{ K}^{-1}$) at 2 T is obviously larger than that of $\text{Gd}(\text{OH})_2\text{Cl}$ ($17.6 \text{ J kg}^{-1} \text{ K}^{-1}$) at 2 T, the volumetric magnetic entropy change of **1** ($92 \text{ mJ cm}^{-3} \text{ K}^{-1}$) at 2 T is close to that of $\text{Gd}(\text{OH})_2\text{Cl}$ ($91 \text{ mJ cm}^{-3} \text{ K}^{-1}$) at 2 T. No obvious difference in the volumetric magnetic entropy change between them is attributed to that the crystal density of **1** is significantly smaller than that of $\text{Gd}(\text{OH})_2\text{Cl}$. In this sense, the introduction of heavy atoms into gadolinium hydroxyl compounds is beneficial to improving their volumetric magnetic entropy change when their magnetic density and magnetic interaction are close.

Table 1. Weiss constants and magnetic entropy changes for selected Gd-based magnetocaloric materials ($-\Delta S_m$).

Compound	θ	$-\Delta S_m/$ $\text{J kg}^{-1} \text{ K}^{-1}$ ($\text{mJ cm}^{-3} \text{ K}^{-1}$)		Ref.
		7 T	2 T	
GdF_3	+0.7	71.6 (506) *	45.5 (322)	[12]
$\text{Gd}(\text{HCOO})_3$	−0.3	55.9 (216) *	43.7 (169) *	[8]
$\text{Gd}(\text{OH})\text{CO}_3$	−1.05	66.4 (355) *	33.7 (180)	[10]
$\text{Gd}(\text{OH})_3$	−1.69	62.0 (346)	26.9 (150)	[9]
$\text{Gd}(\text{OH})_2\text{Cl}$	−1.99	61.8 (319)	17.6 (91)	[33]
$\text{Gd}_3(\text{OH})_8\text{Cl}$	−2.78	59.8 (310)	14.2 (74)	[33]
$[\text{Gd}_3(\text{CO}_3)(\text{OH})_6]\text{OH}$	−4.37	61.5 (262)	10.1 (43)	[42]
$\text{Gd}_2(\text{OH})_5\text{Cl}\cdot 1.5\text{H}_2\text{O}$	−3.1	51.9 (/) *	/	[43]
$\text{Gd}_4(\text{OH})_4(\text{SO}_4)_4(\text{H}_2\text{O})_4$	−1.57	51.3 (199)	25.5 (99)	[44]
$[\text{Gd}_{60}]$	−3.71	48.0 (133)	12.7 (35)	[15]
1	−2.25	59.8 (221)	24.8 (92)	This
2	−2.78	57.6 (293)	15.1 (77)	Work

*: Maximum value in current magnetic field.

3. Conclusions

In summary, we reported on the crystal structures and MCE of the two magnetic refrigeration reagents **1** and **2**. Magnetic study reveals that **1** and **2**, respectively, exhibit magnetic entropy changes of $59.8 \text{ J kg}^{-1} \text{ K}^{-1}$ and $57.6 \text{ J kg}^{-1} \text{ K}^{-1}$ at $T = 2 \text{ K}$ and $\Delta H = 7 \text{ T}$. Significantly, the magnetic entropy changes of $24.8 \text{ J kg}^{-1} \text{ K}^{-1}$ for **1** and $15.1 \text{ J kg}^{-1} \text{ K}^{-1}$ for **2** at $T = 2 \text{ K}$ and $\Delta H = 2 \text{ T}$ exceed most gadolinium hydroxyl compounds, indicating that magnetic refrigerants with large MCE at low fields can be obtained by introducing more weak magnetic exchange ligands to replace hydroxyl groups in gadolinium hydroxyl compounds when the magnetic density remains unchanged.

4. Materials and Methods

4.1. General Information

All materials and reagents were commercially available and used without further purification.

Powder X-ray diffraction data (PXRD) was collected on a Rigaku Ultima IV powder X-ray diffractometer ($\text{Cu K}\alpha$, $\lambda = 1.54184 \text{ \AA}$) in the 2θ range of $5\text{--}60^\circ$ at room temperature. Thermogravimetric analysis (TGA) curve was conducted on an SDT_Q600 thermal analyzer at a rate of $10 \text{ }^\circ\text{C}$ per minute up to $800 \text{ }^\circ\text{C}$ under a constant nitrogen gas. Elemental analyses were carried out using a CE Instruments EA 1110 elemental analyzer. Magnetic measurement was carried out using a Quantum Design MPMS-XL5 superconducting quantum interference device (SQUID).

4.2. Synthesis of $\text{Gd}_5(\text{C}_4\text{O}_4)(\text{HCOO})_3(\text{CO}_3)_2(\text{OH})_6\cdot 2.5\text{H}_2\text{O}$ (**1**)

Compound **1** was prepared by a mixture of $\text{GdCl}_3\cdot 6\text{H}_2\text{O}$ (0.186 g, 0.5 mmol) and squaric acid (0.057 g, 0.5 mmol) dissolved in the mixed solvent of 5 mL *N,N*-dimethylformamide (DMF)

and 5 mL deionized water. The resulting solution was stirred for 30 min before transferred into a Teflon-lined autoclave at 170 °C for 4 days and cooled down to room temperature at a rate of 3 °C h⁻¹. Colorless crystals were obtained in 54% yield based on Gd³⁺. Elem. anal. Calculated (found): C, 8.31% (8.85%); H, 0.93% (0.61%).

4.3. Synthesis of Gd₂(OH)₄SO₄ (2)

Compound **2** was synthesized by a mixture of Gd(NO₃)₃·6H₂O (0.226 g, 0.5 mmol) and ammonium carbonate (0.144 g, 1.5 mmol) dissolved in 5 mL deionized water. An amount of 10 µL concentrated sulfuric acid was introduced into the solution while stirring. The resulting solution was stirred for another 30 min before being transferred into a Teflon-lined autoclave at 250 °C for 3 days and cooled down to room temperature at a rate of 3 °C h⁻¹. Colorless crystals were obtained in 72% yield based on Gd³⁺. Elem. anal. Calculated (found): H, 0.84% (0.59%).

4.4. X-ray Crystallographic Analysis of **1** and **2**

Single crystal data of **1** and **2** were collected by a Rigaku XtaLAB Synergy diffractometer with monochromatic Cu Kα radiation (λ = 1.54184 Å). Data reduction and absorption correction were applied by using the multi-scan program. The structures were determined and refined using full matrix least squares based on *F*² with SHELXS and SHELXL [45] within Olex2 [46]. All non-hydrogen atoms were refined anisotropically. CCDC numbers 2164597 and 2164596 contain the supplementary crystallographic data for this paper. These data can be obtained free of charge via <http://www.ccdc.cam.ac.uk/conts/retrieving.html>. (Accessed on 24 June 2022)

4.5. The Bond Valence Sum (BVS) Analysis of **1** and **2**

The bond valence sum (BVS) analysis was used to determine the oxidation states of oxygen atoms in compound **1** and **2**. The calculation formula is $S_{ij} = \exp[(R_0 - R_{ij})/b]$, in which S_{ij} is the valence of the individual bond, R_{ij} is the observed bond length, R_0 is a constant depended upon the bonded elements, and b is a constant of 0.37. As shown in Tables S1 and S2, the total BVS values of O atoms are very close to the state of +1, for which we identify the states of all O atoms assigned to hydroxyl groups.

Supplementary Materials: The following supporting information can be downloaded at: <https://www.mdpi.com/article/10.3390/inorganics10070091/s1>, Figure S1: PXRD patterns for **1** and **2**; Figure S2: TGA curve of **1** and **2**; Figures S3 and S4: Asymmetric unit and coordination environment for **1** and **2**; Figure S5: Plot of field-dependent magnetizations at 2–10 K for **1** and **2**; Tables S1 and S2: The bond valence sum (BVS) calculations for oxygen atoms of **1** and **2**; Table S3: Crystal data for **1** and **2**; Tables S4 and S5: The Continuous Shape Measurements (CShM) of **1** and **2**; Tables S6 and S7: Selected bond distances (Å) and bond angles (°) of **1** and **2**.

Author Contributions: Conceptualization, B.-L.L. and Q.-F.X.; validation, B.-L.L. and Q.-F.X.; investigation, B.-L.L.; data curation, B.-L.L.; writing—original draft preparation, B.-L.L.; writing—review and editing, L.-S.L.; supervision, L.-S.Z. All authors have read and agreed to the published version of the manuscript.

Funding: This research was funded by National Natural Science Foundation of China, grant number 21431005, 21721001 and 21971214.

Institutional Review Board Statement: Not applicable.

Informed Consent Statement: Not applicable.

Data Availability Statement: Data available in a publicly accessible repository.

Conflicts of Interest: The authors declare no conflict of interest.

References

1. Warburg, E. Magnetische Untersuchungen. *Ann. Phys.* **1881**, *249*, 141–164. [[CrossRef](#)]
2. Weiss, P.; Piccard, A. Le phénomène magnétocalorique. *J. Phys. Theor. Appl.* **1917**, *7*, 103–109. [[CrossRef](#)]
3. Hornibrook, J.M.; Colless, J.I.; Conway Lamb, I.D.; Pauka, S.J.; Lu, H.; Gossard, A.C.; Watson, J.D.; Gardner, G.C.; Fallahi, S.; Manfra, M.J.; et al. Cryogenic Control Architecture for Large-Scale Quantum Computing. *Phys. Rev. Appl.* **2015**, *3*, 024010. [[CrossRef](#)]
4. Fang, T.T. Missing Matter Found in the Cosmic Web. *Nature* **2018**, *558*, 375–376. [[CrossRef](#)]
5. Shirron, P.J. Design of the PIXIE Adiabatic Demagnetization Refrigerators. *Cryogenics* **2012**, *52*, 140–144. [[CrossRef](#)]
6. Martínez-Pérez, M.-J.; Montero, O.; Evangelisti, M.; Luis, F.; Sesé, J.; Cardona-Serra, S.; Coronado, E. Fragmenting Gadolinium: Mononuclear Polyoxometalate-Based Magnetic Coolers for Ultra-Low Temperatures. *Adv. Mater.* **2012**, *24*, 4301–4305. [[CrossRef](#)]
7. Cho, A. Helium-3 Shortage Could Put Freeze on Low-Temperature Research. *Science* **2009**, *326*, 778–779. [[CrossRef](#)]
8. Lorusso, G.; Sharples, J.W.; Palacios, E.; Roubeau, O.; Brechin, E.K.; Sessoli, R.; Rossin, A.; Tuna, F.; McInnes, E.J.L.; Collison, D.; et al. A Dense Metal–Organic Framework for Enhanced Magnetic Refrigeration. *Adv. Mater.* **2013**, *25*, 4653–4656. [[CrossRef](#)]
9. Yang, Y.; Zhang, Q.-C.; Pan, Y.-Y.; Long, L.-S.; Zheng, L.-S. Magnetocaloric Effect and Thermal Conductivity of Gd(OH)₃ and Gd₂O(OH)₄(H₂O)₂. *Chem. Commun.* **2015**, *51*, 7317–7320. [[CrossRef](#)]
10. Chen, Y.-C.; Qin, L.; Meng, Z.-S.; Yang, D.-F.; Wu, C.; Fu, Z.; Zheng, Y.-Z.; Liu, J.-L.; Tarasenko, R.; Orendáč, M.; et al. Study of a Magnetic-Cooling Material Gd(OH)CO₃. *J. Mater. Chem. A* **2014**, *2*, 9851–9858. [[CrossRef](#)]
11. Palacios, E.; Rodríguez-Velamazán, J.A.; Evangelisti, M.; McIntyre, G.J.; Lorusso, G.; Visser, D.; de Jongh, L.J.; Boatner, L.A. Magnetic Structure and Magnetocalorics of GdPO₄. *Phys. Rev. B* **2014**, *90*, 214423. [[CrossRef](#)]
12. Chen, Y.-C.; Prokleška, J.; Xu, W.-J.; Liu, J.-L.; Liu, J.; Zhang, W.-X.; Jia, J.-H.; Sechovský, V.; Tong, M.-L. A Brilliant Cryogenic Magnetic Coolant: Magnetic and Magnetocaloric Study of Ferromagnetically Coupled GdF₃. *J. Mater. Chem. C* **2015**, *3*, 12206–12211. [[CrossRef](#)]
13. Mukherjee, P.; Wu, Y.; Lampronti, G.I.; Dutton, S.E. Magnetic Properties of Monoclinic Lanthanide Orthoborates, LnBO₃, Ln = Gd, Tb, Dy, Ho, Er, Yb. *Mater. Res. Bull.* **2018**, *98*, 173–179. [[CrossRef](#)]
14. Peng, J.-B.; Kong, X.-J.; Zhang, Q.-C.; Orendáč, M.; Prokleška, J.; Ren, Y.-P.; Long, L.-S.; Zheng, Z.; Zheng, L.-S. Beauty, Symmetry, and Magnetocaloric Effect—Four-Shell Keplerates with 104 Lanthanide Atoms. *J. Am. Chem. Soc.* **2014**, *136*, 17938–17941. [[CrossRef](#)] [[PubMed](#)]
15. Luo, X.-M.; Hu, Z.-B.; Lin, Q.; Cheng, W.; Cao, J.-P.; Cui, C.-H.; Mei, H.; Song, Y.; Xu, Y. Exploring the Performance Improvement of Magnetocaloric Effect Based Gd-Exclusive Cluster Gd₆₀. *J. Am. Chem. Soc.* **2018**, *140*, 11219–11222. [[CrossRef](#)]
16. Chen, W.; Liao, P.; Yu, Y.; Zheng, Z.; Chen, X.; Zheng, Y. A Mixed-Ligand Approach for a Gigantic and Hollow Heterometallic Cage {Ni₆₄RE₉₆} for Gas Separation and Magnetic Cooling Applications. *Angew. Chem. Int. Ed.* **2016**, *55*, 9375–9379. [[CrossRef](#)]
17. Evangelisti, M.; Roubeau, O.; Palacios, E.; Camón, A.; Hooper, T.N.; Brechin, E.K.; Alonso, J.J. Cryogenic Magnetocaloric Effect in a Ferromagnetic Molecular Dimer. *Angew. Chem. Int. Ed.* **2011**, *50*, 6606–6609. [[CrossRef](#)]
18. Liu, S.J.; Zhao, J.P.; Tao, J.; Jia, J.M.; Han, S.D.; Li, Y.; Chen, Y.C.; Bu, X.H. An Unprecedented Decanuclear Gd^{III} Cluster for Magnetic Refrigeration. *Inorg. Chem.* **2013**, *52*, 9163–9165. [[CrossRef](#)]
19. Guo, F.-S.; Chen, Y.-C.; Mao, L.-L.; Lin, W.-Q.; Leng, J.-D.; Tarasenko, R.; Orendáč, M.; Prokleška, J.; Sechovský, V.; Tong, M.-L. Anion-Templated Assembly and Magnetocaloric Properties of a Nanoscale {Gd₃₈} Cage versus a {Gd₄₈} Barrel. *Chem. Eur. J.* **2013**, *19*, 14876–14885. [[CrossRef](#)]
20. Zheng, X.Y.; Jiang, Y.H.; Zhuang, G.L.; Liu, D.P.; Liao, H.G.; Kong, X.J.; Long, L.S.; Zheng, L.S. A Gigantic Molecular Wheel of {Gd₁₄₀}: A New Member of the Molecular Wheel Family. *J. Am. Chem. Soc.* **2017**, *139*, 18178–18181. [[CrossRef](#)]
21. Das, M.; Roy, S.; Mandal, P. Giant Reversible Magnetocaloric Effect in a Multiferroic GdFeO₃ Single Crystal. *Phys. Rev. B* **2017**, *96*, 174405. [[CrossRef](#)]
22. Jia, J.-H.; Ke, Y.-J.; Li, X.; Zhang, H.-R.; Yu, Z.-P.; Cheng, Z.-H.; Zhai, K.; Liu, Z.-Y.; Wang, J.-F. A Large Magnetocaloric Effect of GdCoO_{3-δ} Epitaxial Thin Films Prepared by a Polymer Assisted Spin-Coating Method. *J. Mater. Chem. C* **2019**, *7*, 14970–14976. [[CrossRef](#)]
23. Ashtar, M.; Bai, Y.; Xu, L.; Wan, Z.; Wei, Z.; Liu, Y.; Marwat, M.A.; Tian, Z. Structure and Magnetic Properties of Melilite-Type Compounds RE₂Be₂GeO₇ (RE = Pr, Nd, Gd–Yb) with Rare-Earth Ions on Shastry–Sutherland Lattice. *Inorg. Chem.* **2021**, *60*, 3626–3634. [[CrossRef](#)] [[PubMed](#)]
24. Xu, L.-Y.; Zhao, J.-P.; Liu, T.; Liu, F.-C. Gadolinium Sulfate Modified by Formate to Obtain Optimized Magneto-Caloric Effect. *Inorg. Chem.* **2015**, *54*, 5249–5256. [[CrossRef](#)]
25. Tang, Q.; Yang, Y.-L.; Zhang, N.; Liu, Z.; Zhang, S.-H.; Tang, F.-S.; Hu, J.-Y.; Zheng, Y.-Z.; Liang, F.-P. A Multifunctional Lanthanide Carbonate Cluster Based Metal–Organic Framework Exhibits High Proton Transport and Magnetic Entropy Change. *Inorg. Chem.* **2018**, *57*, 9020–9027. [[CrossRef](#)]
26. Biswas, S.; Mondal, A.K.; Konar, S. Densely Packed Lanthanide Cubane Based 3D Metal–Organic Frameworks for Efficient Magnetic Refrigeration and Slow Magnetic Relaxation. *Inorg. Chem.* **2016**, *55*, 2085–2090. [[CrossRef](#)]
27. Brown, I.D.; Altermatt, D. Bond-Valence Parameters Obtained from a Systematic Analysis of the Inorganic Crystal Structure Database. *Acta Cryst. B* **1985**, *41*, 244–247. [[CrossRef](#)]
28. Alvarez, S.; Alemany, P.; Casanova, D.; Cirera, J.; Llunell, M.; Avnir, D. Shape Maps and Polyhedral Interconversion Paths in Transition Metal Chemistry. *Coord. Chem. Rev.* **2005**, *249*, 1693–1708. [[CrossRef](#)]

29. Biswas, S.; Jena, H.S.; Adhikary, A.; Konar, S. Two Isostructural 3D Lanthanide Coordination Networks (Ln = Gd³⁺, Dy³⁺) with Squashed Cuboid-Type Nanoscopic Cages Showing Significant Cryogenic Magnetic Refrigeration and Slow Magnetic Relaxation. *Inorg. Chem.* **2014**, *53*, 3926–3928. [[CrossRef](#)]
30. Huang, Y.-T.; Lai, Y.-C.; Wang, S.-L. Intrinsic Green Phosphor Containing a {Y₅O₂₂} Pentamer Unit and a Carbonate Ligand Generated In Situ from Squaric Acid. *Chem. Eur. J.* **2012**, *18*, 8614–8616. [[CrossRef](#)]
31. Liang, J.; Ma, R.; Geng, F.; Ebina, Y.; Sasaki, T. Ln₂(OH)₄SO₄·nH₂O (Ln = Pr to Tb; n ~ 2): A New Family of Layered Rare-Earth Hydroxides Rigidly Pillared by Sulfate Ions. *Chem. Mater.* **2010**, *22*, 6001–6007. [[CrossRef](#)]
32. Wang, X.; Molokeev, M.S.; Zhu, Q.; Li, J.-G. Controlled Hydrothermal Crystallization of Anhydrous Ln₂(OH)₄SO₄ (Ln = Eu–Lu, Y) as a New Family of Layered Rare Earth Metal Hydroxides. *Chem. Eur. J.* **2017**, *23*, 16034–16043. [[CrossRef](#)] [[PubMed](#)]
33. Wang, Y.; Qin, L.; Zhou, G.-J.; Ye, X.; He, J.; Zheng, Y.-Z. High-Performance Low-Temperature Magnetic Refrigerants Made of Gadolinium–Hydroxy–Chloride. *J. Mater. Chem. C* **2016**, *4*, 6473–6477. [[CrossRef](#)]
34. Gschneidner, K.A., Jr.; Pecharsky, V.K.; Tsokol, A.O. Recent Developments in Magnetocaloric Materials. *Rep. Prog. Phys.* **2005**, *68*, 1479–1539. [[CrossRef](#)]
35. Pecharsky, V.; Gschneidner, K.; Pecharsky, A.; Tishin, A. Thermodynamics of the Magnetocaloric Effect. *Phys. Rev. B* **2001**, *64*, 144406. [[CrossRef](#)]
36. de Oliveira, N.A.; von Ranke, P.J. Magnetocaloric Effect around a Magnetic Phase Transition. *Phys. Rev. B* **2008**, *77*, 214439. [[CrossRef](#)]
37. Evangelisti, M.; Brechin, E.K. Recipes for Enhanced Molecular Cooling. *Dalton Trans.* **2010**, *39*, 4672–4676. [[CrossRef](#)]
38. Shirron, P.J. Applications of the Magnetocaloric Effect in Single-Stage, Multi-Stage and Continuous Adiabatic Demagnetization Refrigerators. *Cryogenics* **2014**, *62*, 130–139. [[CrossRef](#)]
39. Shirron, P.J.; Canavan, E.R.; DiPirro, M.J.; Tuttle, J.G.; Yeager, C.J. A Multi-Stage Continuous–Duty Adiabatic Demagnetization Refrigerator. In *Advances in Cryogenic Engineering*; Shu, Q.S., Ed.; Springer: Boston, MA, USA, 2000; pp. 1629–1638.
40. Sagawa, M.; Fujimura, S.; Togawa, N.; Yamamoto, H.; Matsuura, Y. New Material for Permanent Magnets on a Base of Nd and Fe (Invited). *J. Appl. Phys.* **1984**, *55*, 2083–2087. [[CrossRef](#)]
41. You, C.Y.; Ping, D.H.; Hono, K. Magnetic Properties and Microstructure of Fe₃B/Pr₂Fe₁₄B–Type Nanocomposite Magnets with Co and Cr Additions. *J. Magn. Magn. Mater.* **2006**, *299*, 136–144. [[CrossRef](#)]
42. Dong, J.; Cui, P.; Shi, P.-F.; Cheng, P.; Zhao, B. Ultrastrong Alkali-Resisting Lanthanide-Zeolites Assembled by [Ln₆₀] Nanocages. *J. Am. Chem. Soc.* **2015**, *137*, 15988–15991. [[CrossRef](#)] [[PubMed](#)]
43. Abellán, G.; Espallargas, G.M.; Lorusso, G.; Evangelisti, M.; Coronado, E. Layered Gadolinium Hydroxides for Low–Temperature Magnetic Cooling. *Chem. Commun.* **2015**, *51*, 14207–14210. [[CrossRef](#)] [[PubMed](#)]
44. Han, S.-D.; Miao, X.-H.; Liu, S.-J.; Bu, X.-H. Magnetocaloric Effect and Slow Magnetic Relaxation in Two Dense (3,12)–Connected Lanthanide Complexes. *Inorg. Chem. Front.* **2014**, *1*, 549–552. [[CrossRef](#)]
45. Sheldrick, G.M. Crystal Structure Refinement with SHELXL. *Acta Cryst. C Struct. Chem.* **2015**, *71*, 3–8. [[CrossRef](#)]
46. Dolomanov, O.V.; Bourhis, L.J.; Gildea, R.J.; Howard, J.A.K.; Puschmann, H. OLEX2: A Complete Structure Solution, Refinement and Analysis Program. *J. Appl. Crystallogr.* **2009**, *42*, 339–341. [[CrossRef](#)]